Available online at www.sciencedirect.com

jmr&t Journal of Materials Research and Technology

journal homepage: www.elsevier.com/locate/jmrt

Original Article

Effect of combined lean additions of isomorphous and eutectoid beta stabilisers on the properties of titanium

L. Bolzoni[*], *M. Paul*, *F. Yang*

The University of Waikato, Hamilton 3240, New Zealand

ARTICLE INFO

Article history:
Received 11 September 2022
Accepted 3 November 2022
Available online 8 November 2022

Keywords:
Titanium alloys
Powder metallurgy
Blended elemental
Homogeneous microstructure
Mechanical properties

ABSTRACT

Reduction of the manufacturing cost of titanium and the development of new alloys are crucial to effectively harvest the benefits derived by the use of titanium in industrial applications. Therefore, we considered the creation of new Ti-2X-2Z alloys via the combined lean additions of isomorphous (i.e. Nb) and eutectoid (i.e. Cu, Mn, and Fe) beta stabilisers, and systematically analysed their effect on the manufacturability and mechanical response of titanium produced via powder metallurgy. It is found that the addition of the alloying elements reduces the compressibility of the powder blend but enhances the densification. The microstructure of titanium is transformed into a Widmanstätten structure composed of α grain boundaries and $\alpha+\beta$ lamellae where the stronger the beta stabilisers the more refined the microstructural features, and no intermetallic phases are precipitated despite the use of eutectoid stabilisers. Consequently, the combined addition of isomorphous and eutectoid beta stabilisers has a significant effect on the mechanical response with the material becoming stronger, harder and less tough with the increment of the potency of the added beta stabilisers; however, the Ti-2X-2Z alloys share similar strengthening mechanisms. A more accurate theoretical equation for developing titanium alloys through the molybdenum equivalent parameter should be developed.

1. Introduction

Titanium (Ti) and its alloys are characterised by a combination of properties such as low density, high strength, good corrosion resistance, biocompatibility, and mechanical properties at relatively high temperatures better suited, with respect to competitors' metals [1,2], for most structural engineering applications. However, the widespread application of Ti alloys in industry is hindered by the high costs involved in the extraction and fabrication of Ti as a consequence of the high reactivity with atmospheric gases, especially oxygen, and the poor machinability. Consequently, Ti alloys are still primarily used in high demanding engineering sectors such as the aeronautic, the biomedical, and the petrochemical where the high cost is overbalanced by the benefits brought about by using Ti alloys rather than any other of the available structural metals. With respect to the fabrication of Ti alloys, powder metallurgy, a

* Corresponding author.
E-mail address: bolzoni.leandro@gmail.com (L. Bolzoni).
https://doi.org/10.1016/j.jmrt.2022.11.023

recognised green technology, has been identified as an ideal alternative manufacturing technique for Ti alloys when aiming to reduce their cost. This is because the fabrication of Ti alloys via powder metallurgy entails advantages such as solid-state processing (i.e. limiting the reactivity of Ti), reduced number of operations needed to obtain the product with the final desired geometry (i.e. near-net-shape processing), and high yield of material (i.e. waste minimisation during fabrication). Furthermore, powder metallurgy offers the possibility to design new chemical compositions not otherwise achievable and the ability to easily tailor the performance of Ti, especially when the composition is created through the so-called blended elemental approach where elemental powders of the desired elements are mixed together to make up the desired composition [1].

Ti is an allotropic metal and it has two main equilibrium phases, the low temperature hexagonal close packed (HCP) alpha Ti and the high temperature body-centred cubic (BCC) beta Ti phases. The addition of each alloying element either increases or decreases the allotropic phase transformation temperature and, therefore, the alloying elements are known as α or β stabilisers, respectively. This entails the fact that if enough β stabilisers are added (worth to note that do exit isomorphous and eutectoid β stabilising elements), the high temperature beta Ti phase is stabilised at room temperature. Accordingly, Ti alloys are classified as α, α+β, and β alloys depending on the phases present in the microstructure of the alloy at room temperature after an annealing heat treatment. It is worth mentioning that there are also near-α alloys, which generally have a maximum of 2–3% of β stabilisers added in their composition (all compositions are in wt.% unless specified differently), and β Ti alloys are further subdivided into metastable and fully stable alloys depending on the total amount of β stabilisers present. α Ti alloys are best known for their high strength and corrosion resistance, α+β Ti alloys for their balance of mechanical performance including strength and toughness, and β Ti alloys for their enhanced formability [3,4].

The design of new Ti alloy compositions, which can be used to reduce the intrinsic cost of Ti via the addition of cheap alloying elements such as Fe, can be tackled using different strategies, two of which are the bond order/d-orbital energy (B_o-M_d) map [5,6] and the molybdenum equivalent (MoE) parameter [7,8]. The latter is preferred for its simplicity where the stabilisation effect on the β-Ti phase of each alloying element to be added in the composition is accounted for through a weighting factor. Currently, in literature there are at least two definitions of the MoE parameter, respectively shown in Eq. (1) [7] and Eq. (2) [8], which are also used to classify Ti alloys. The weighting factors of these equations are for compositions in wt.% and were obtained in quenched alloys.

$$MoE(1) = 1.0\,Mo + 0.67\,V + 0.44\,W + 0.28\,Nb + 0.22\,Ta + 2.9\,Fe + 1.6\,Cr + 0.77\,Cu + 1.11\,Ni + 1.43\,Co + 1.54\,Mn - 1.0\,Al \quad \text{(Eq. 1)}$$

$$MoE(2) = 1.0\,Mo + 1.25\,V + 0.59\,W + 0.28\,Nb + 0.22\,Ta + 1.93\,Fe + 1.84\,Cr + 1.50\,Cu + 2.46\,Ni + 2.67\,Co + 2.26\,Mn + 0.30\,Sn + 0.47\,Zr + 3.01\,Si - 1.47\,Al \quad \text{(Eq. 2)}$$

Among β stabilisers, Nb is an isomorphous β stabiliser used because of its non-toxic behaviour and ability to lower the elastic modulus, Cu is a eutectoid β stabiliser used to provide antibacterial capability and burn resistance, Mn is a strong eutectoid β stabiliser used to reduce the cost and because of its lower toxicity than V [9,10], and Fe is a strong eutectoid β stabiliser primarily used to reduce the intrinsic cost of the alloy and enhance the mechanical behaviour. The addition of Nb [11–17], Cu [18–28] and Fe [29–35] in their respective binary Ti–Nb, Ti–Cu and Ti–Fe systems has been widely investigated whilst the addition of Mn in binary Ti–Mn alloys has been much less explored [36–39].

Studies reporting the processing and properties of ternary alloys where the combination of any two of those elements (i.e. Nb, Cu, Mn, and Fe) were jointly added to Ti are also much more uncommon and have specific limitations. In particular, to the best knowledge of the authors, few studies reported ternary Ti-xNb-yCu alloys [40–42], but only considering high Nb + Cu contents (i.e. $\geq$ 10%) and primarily using casting as manufacturing process. Two studies analysed ternary Ti-xNb-xMn alloys [43,44], but with the composition of one of two elements fixed and no characterisation of the alloys in the as-obtained conditions was performed, as the alloys were always heat treated. Ternary Ti-xNb-yFe alloys have been slightly more investigated [45–52] but, as for ternary Ti-xNb-xMn alloys, most literature investigated alloys where the content of one of the two alloying elements was kept constant, focused on obtaining metastable or stable β Ti alloys (i.e. high Nb + Fe contents), and wrought metallurgy was the prime processing choice. There are few reports on ternary Ti-xFe-yCu alloys [53–56], but only the work of Zadorozhnyy et al. [54,55] actually considered the development of α+β alloys, even though they only analysed one particular composition (i.e. Ti-3.5Fe-3.9Cu), and there is no literature on manufacturing ternary Ti-xFe-yCu alloys via powder metallurgy. Only Ikeda et al. [57] studied ternary Ti-xFe-yMn, but once again only alloys with high addition rates resulting in materials with a microstructure composed of equiaxed beta grains were analysed. It is also worth mentioning that not many of the previously mentioned studies quantified the structural behaviour of the ternary alloys, and if they did, not many reported tensile properties.

The aim of this work is thus to understand the effect that combined lean additions of isomorphous (i.e. Nb) and eutectoid (i.e. Cu, Mn, and Fe) beta stabilisers have on the manufacturing and mechanical behaviour of Ti. In particular, the amount of each alloying element was fixed at 2% and, therefore, the following Ti-2X-2Z alloys were investigated: Ti–2Nb–2Cu, Ti–2Nb–2Mn, Ti–2Nb–2Fe, Ti–2Fe–2Cu, and Ti–2Fe–2Mn. CP-Ti (commercially pure) was also analysed as the reference material. The alloys were produced via powder metallurgy and their mechanical and strengthening behaviour based on tensile testing was quantified.

2. Experimental procedure

SEM micrographs showing the morphology and basic features of the elemental powders used as raw materials for the current study are reported, respectively, in Fig. 1 and Table 1. It can be seen that both Ti and Nb have irregular morphology, Cu

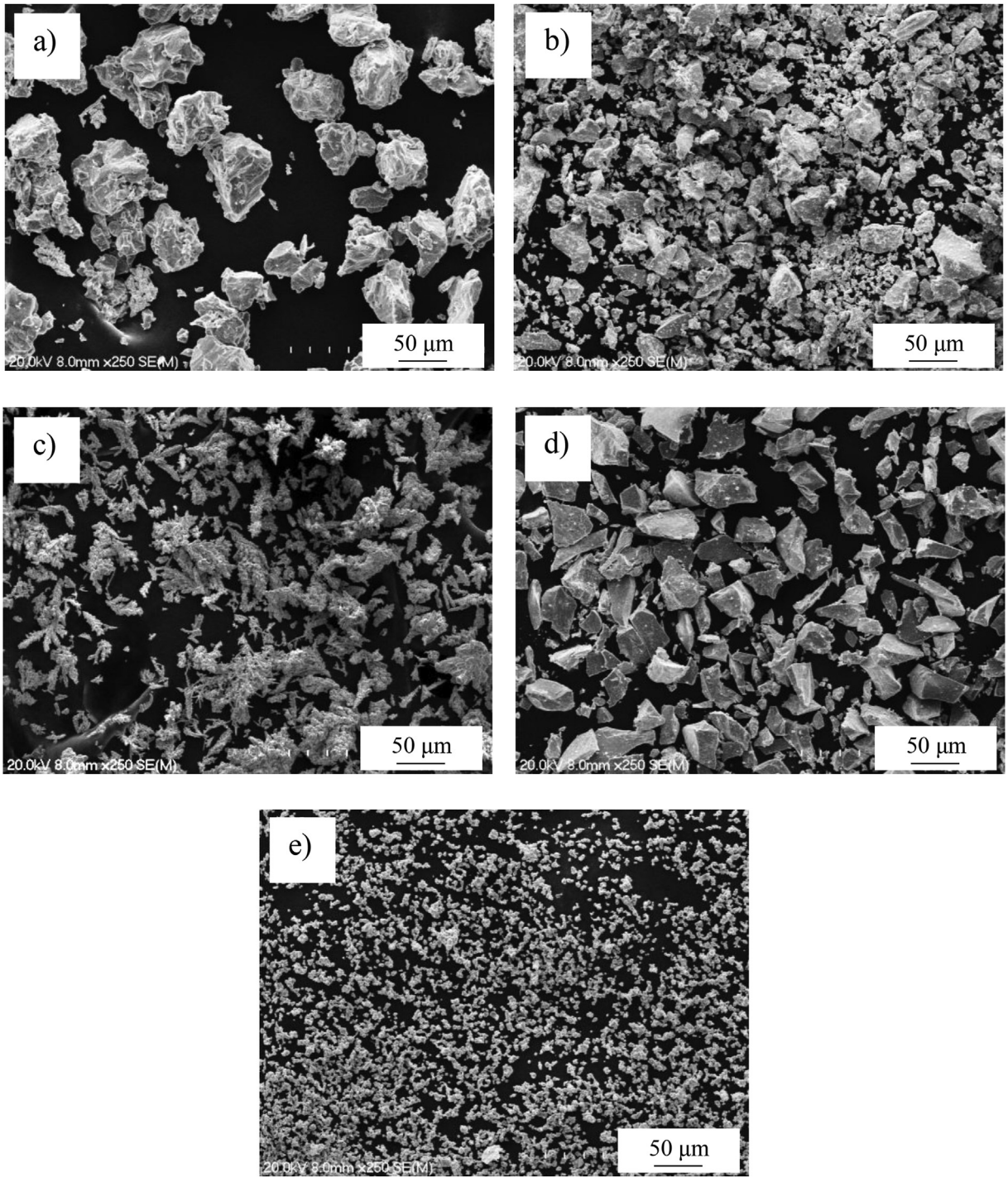

Fig. 1 – SEM micrographs showing the morphology of the raw materials: a) irregular Ti powder, b) irregular Nb powder, c) dendritic Cu powder, d) angular Mn powder, and e) spherical Fe powder.

is dendritic, Mn is angular, and Fe is spherical. The maximum particle size is slightly different for each powder and Ti, which constitutes the bulk of the material, has the biggest particle size ($D_{90} < 75$ μm), which is ideal for its processing via powder metallurgy.

The correct amount of raw powders were weighted and mixed for 30 min using a revolution frequency of 45 Hz. The blends of mixed powders were then compacted into 40 mm cylindrical samples at room temperature via applying a

Table 1 – Suppliers' specification of the raw materials.

Powder	Purity [%]	Maximum particle size [μm/mesh]	Supplier
Ti	99.4	75/200	GoodFellow
Nb	99.8	45/325	AlfaAesar
Cu	99.7	63/230	Merck KGaA
Mn	99.0	45/325	Sigma-Aldrich
Fe	99.0	10/1200	GoodFellow

uniaxial pressing of 600 MPa by means of a hydraulic press. Vacuum sintering of the pressed compacts was performed at 1300 °C using a dwell time of 120 min, a heating rate of 10 °C/min, and furnace cooling under vacuum.

The theoretical density of the alloys was calculated by means of the rule of mixtures. The density of the pressed compacts was calculated as the mass-to-volume ratio for which 5 measurements of the thickness and 3 measurements of the dimeter were taken using a 2-decimal digital calliper. The weight was quantified by means of a 4-decimal analytical balance. Phase analysis by means of X-ray diffraction was done on a Philips X'pert with Cu K_{α} radiation using a scanning angle range of 25–65°, and a step size of 0.013°. Microstructural characterisation was performed with both optical (Olympus BX53) and electronic (Hitachi S4700) microscopes for which the samples were metallographically prepared using the standard grinding and polishing method and final chemical etching by means of a water-based Kroll solution (2 vol% HF and 4 vol% HNO_3).

The mechanical behaviour of the alloys was quantified measuring quasi-static tensile properties and hardness. In particular, an Instron 33R4204 universal tester equipped with an external mechanical extensometer was run at a strain rate of $5 \cdot 10^{-3}$ 1/s to test a minimum of five dogbone samples with cross-section of 2 × 2 mm^2 and gage length of 20 mm. A universal hardness tester was used to measure the Rockwell hardness (HRA) of the alloys.

3. Results

Fig. 2 summarises the measurements of the physical properties of the Ti-2X-2Z alloys, which include theoretical, green, and sintered density as well as densification and porosity. The theoretical density of the Ti-2X-2Z alloys is higher than that of CP-Ti (i.e. 4.51 g/cm^3) and ranges from 4.64 g/cm^3 for the Ti–2Fe–2Mn alloy to 4.68 g/cm^3 for the Ti–2Nb–2Cu alloy. The sintered density of the Ti-2X-2Z alloys is also higher compared

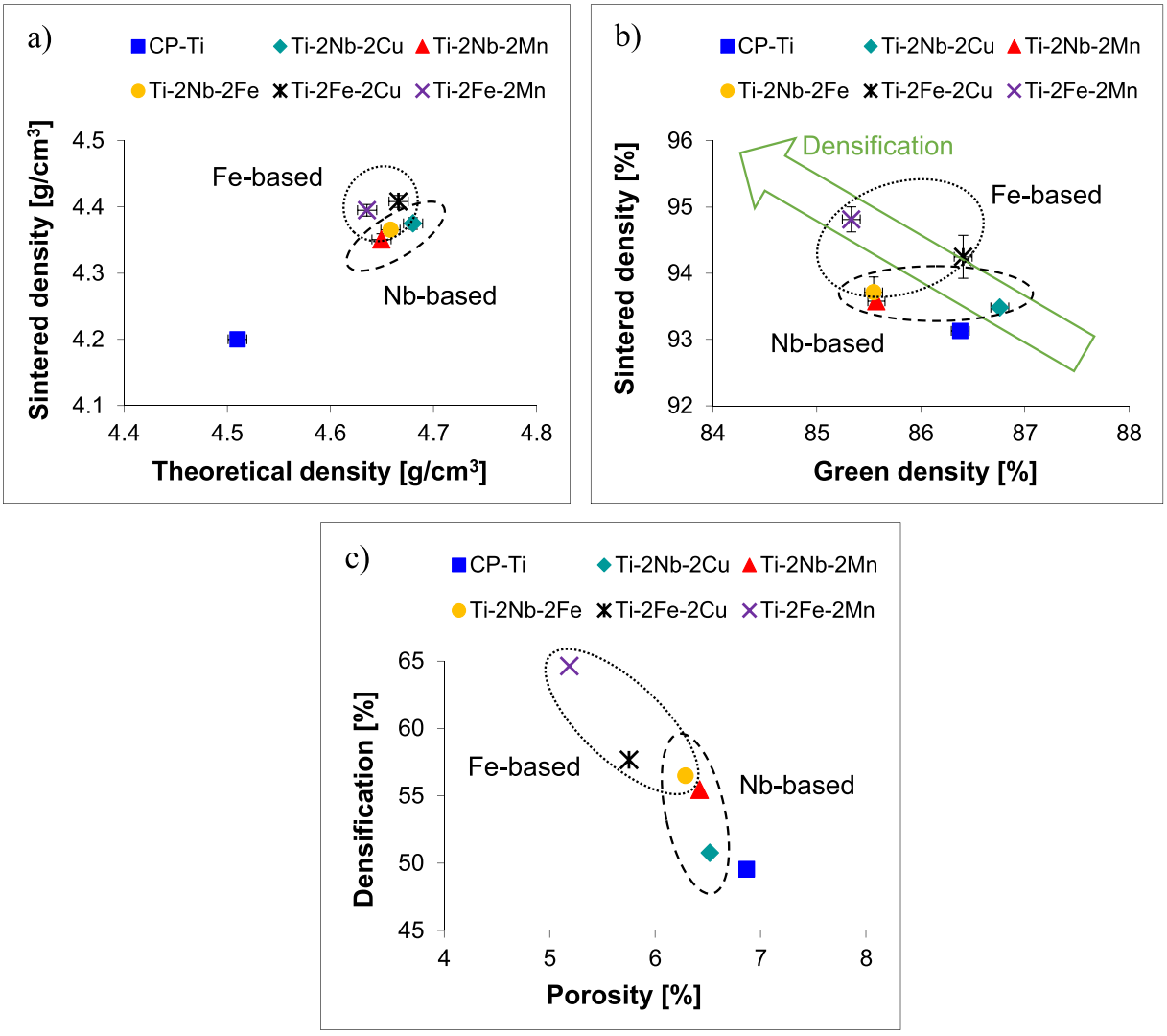

Fig. 2 – Variation of the physical properties of the Ti-2X-2Z alloys: a) sintered density vs. theoretical density, b) sintered density vs. green density, and c) densification vs. porosity.

to CP-Ti where Nb-based Ti-2X-2Z alloys (i.e. Ti–2Nb–2Cu, Ti–2Nb–2Mn, and Ti–2Nb–2Fe) show a linear relationship between sintered and theoretical density, which is not the case for the Fe-based Ti-2X-2Z alloys (i.e. Ti–2Nb–2Fe, Ti–2Fe–2Cu, and Ti–2Fe–2Mn). Considering the relative green density (Fig. 2b), the Ti–2Nb–2Cu alloy (86.8%) has a higher value compared to CP-Ti (86.4%), the Ti–2Fe–2Cu alloy has the same value (86.4%) of CP-Ti, whereas all the other alloys have lower green density (i.e. 85.3–85.6%) in comparison to CP-Ti. However, the values of the relative sintered density of the Ti-2X-2Z alloys (93.5–94.8%) are all greater than that of CP-Ti (93.1%). The values of the relative sintered density of the Ti-2X-2Z alloys are comparable to those of other Ti-based materials manufactured by press and sinter [15,27,29,30,38,44,58]. From Fig. 2c), it can be seen that the Ti-2X-2Z alloys have, thus, lower amount of residual porosity (5.2–6.5%) compared to CP-Ti (6.9%) due to the higher densification (50.8–64.6%) promoted by the addition of the alloying elements to CP-Ti, which has a densification of 49.6%.

The results of the XRD analysis carried out on the Ti-2X-2Z alloys are shown in Fig. 3. It is worth mentioning that the plane/family of planes of the different phases were labelled only the first time encountered. As expected, the alpha Ti phase with HCP structure (a = 2.95 Å and c = 4.67 Å) was the only phase detected for CP-Ti. The alpha Ti phase was also the only phase detected for the Ti–2Nb–2Cu and Ti–2Fe–2Cu

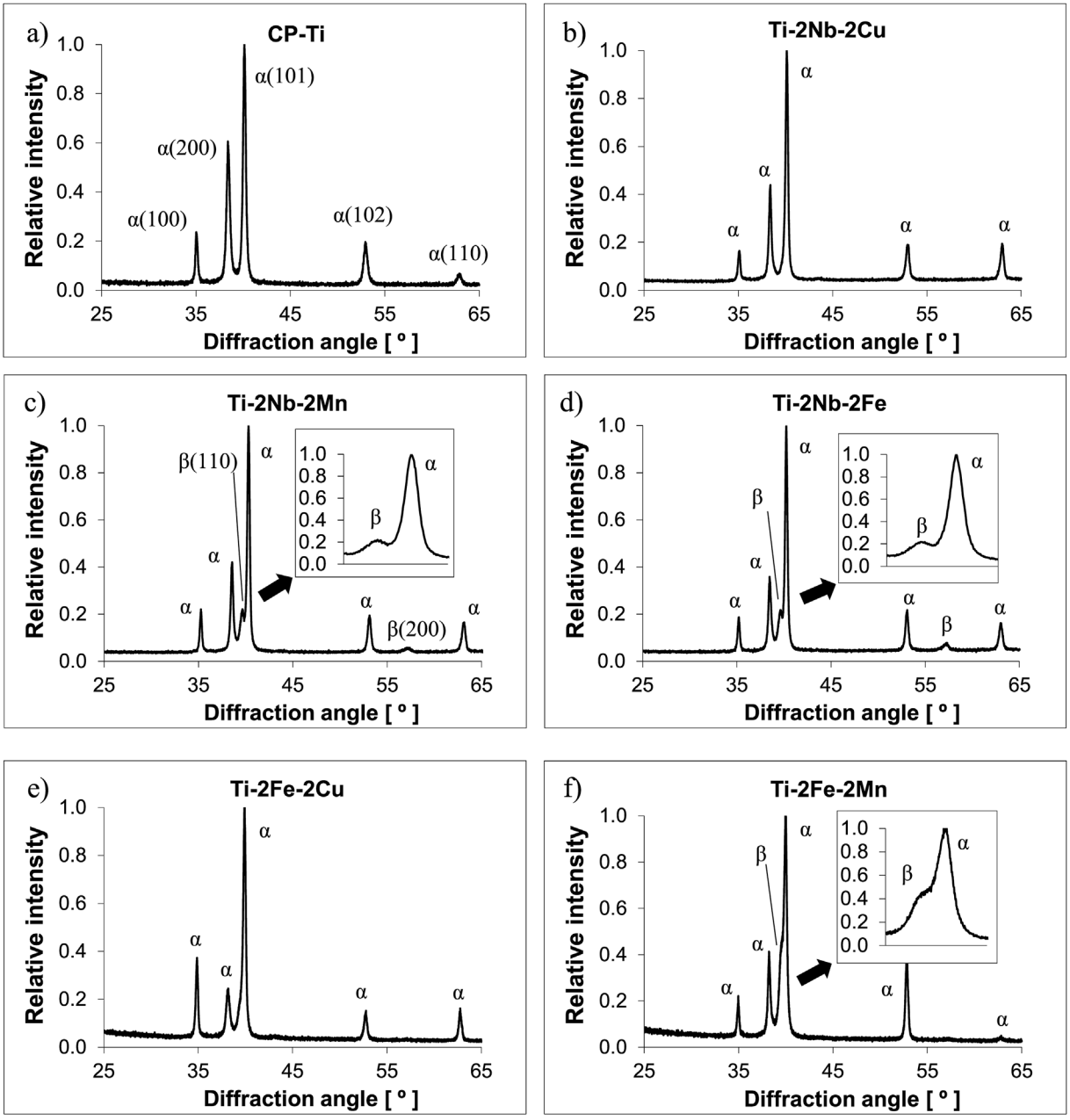

Fig. 3 – Results of the XRD analysis of the Ti-2X-2Z alloys: a) CP-Ti, b) Ti–2Nb–2Cu, c) Ti–2Nb–2Mn, d) Ti–2Nb–2Fe, e) Ti–2Fe–2Cu, and f) Ti–2Fe–2Mn.

alloys whereas both the alpha Ti and beta Ti with BCC structure (a = 3.30 Å) phases were detected for the other Ti-2X-2Z alloys.

Fig. 4 shows representative micrographs of the microstructure of the Ti-2X-2Z alloys analysed at low magnification via optical microscopy and at high magnification by means of scanning electron microscopy, respectively. In terms of microstructure, CP-Ti is composed of Widmanstätten α plates whilst the Ti-2X-2Z alloys have a Widmanstätten microstructure, independently of their actual chemical composition. The primary differences between the Widmanstätten structures of the Ti-2X-2Z alloys is the size of the α+β lamellae found within the α grains, and the morphology of the α grain boundaries (or prior β grains), which is elongated in the case of the Cu-containing Ti-2X-2Z alloys (i.e. Ti–2Nb–2Cu and Ti–2Fe–2Cu) and equiaxed for the rest of the Ti-2X-2Z alloys. The optical micrographs show that, regardless of the chemistry of the alloy, CP-Ti and the Ti-2X-2Z alloys are characterised by a uniform distribution of isolated spherical residual pores left by the sintering process [59]. The volumetric amount of residual pores (~5–7%) agrees with the results presented in Fig. 2.

The variation of the mechanical properties of the Ti-2X-2Z alloys is presented in Fig. 5 where, from the representative tensile curves, it can be seen that both CP-Ti and the Ti-2X-2Z alloys are characterised by both elastic and plastic deformation before failure, which does not happen catastrophically. The lean addition of the selected alloying elements has a profound impact on the tensile behaviour as the Ti-2X-2Z alloys all have much higher strength and lower ductility with respect to CP-Ti. Specifically, the lowest strength and hardness and the highest elongation are found in CP-Ti, and the highest strength and hardness and lowest elongation in the Ti–2Fe–2Mn alloy. More in detail, the ultimate tensile strength varies between 447 ± 23 MPa to 676 ± 16 MPa and, consequently, the hardness increases from 50 ± 0.7 to 59 ± 1.2 HRA (Fig. 5b). Moreover, the yield stress varies between 371 ± 31 MPa to 606 ± 6 MPa and, consequently, the elongation decreases from 14.4 ± 1.1 to 2.7 ± 0.9 (Fig. 5c).

Fig. 6 shows representative fractographic micrographs of the Ti-2X-2Z alloys where it can be seen that the fracture surface of the Ti-2X-2Z alloys is, generally, rougher with respect to that of CP-Ti. The latter failed in a ductile way due to the transgranular fracture at the Widmanstätten α plates whilst the Ti-2X-2Z alloys mainly failed in a ductile way through a combined transgranular and intergranular fracture of the α and β phase, respectively. Most of the residual pores are deformed as they contributed to the failure of the Ti-2X-2Z alloys.

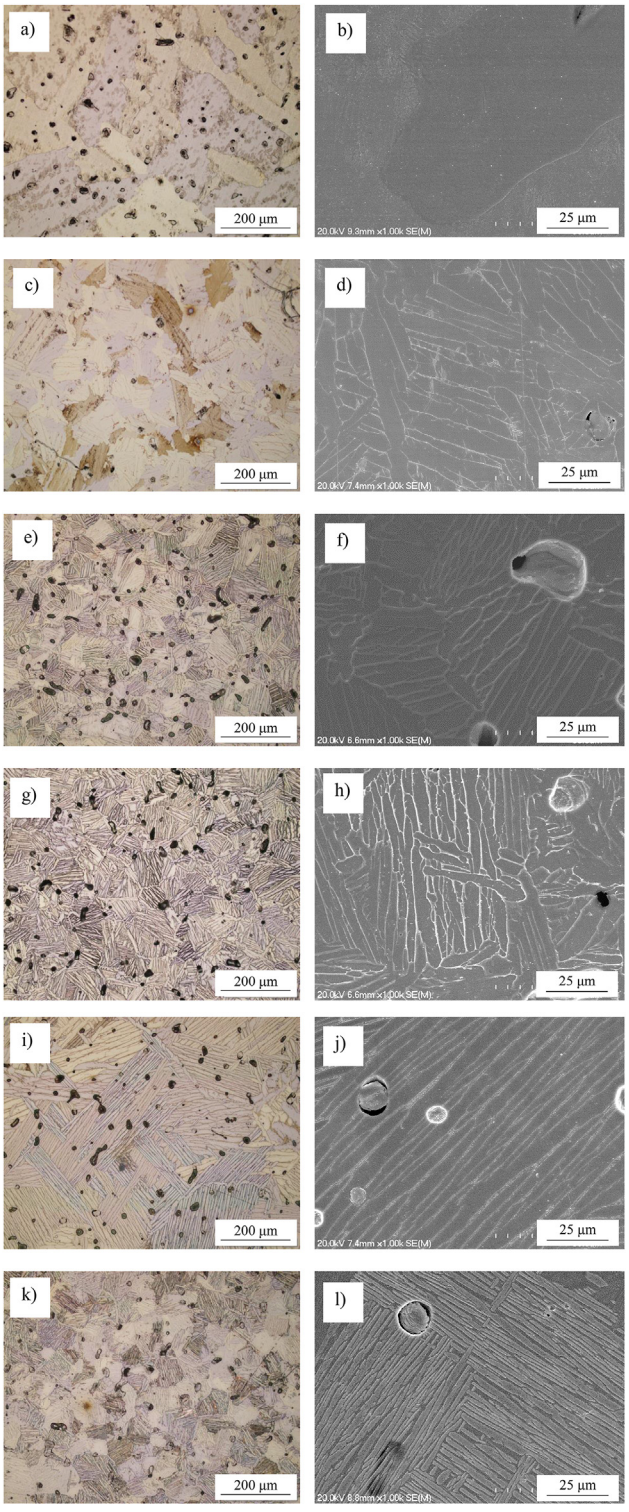

Fig. 4 – Representative low (i.e. optical) and high (i.e. SEM) magnification micrographs, respectively, of the Ti-2X-2Z alloys: a-b) CP-Ti, c-d) Ti–2Nb–2Cu, e-f) Ti–2Nb–2Mn, g-h) Ti–2Nb–2Fe, i-j) Ti–2Fe–2Cu, and k-l) Ti–2Fe–2Mn.

4. Discussion

In this study, Ti-2X-2Z alloys were designed based on lean additions of isomorphous and eutectoid beta stabilisers keeping the ratio of the two alloying elements constant. The new Ti-2X-2Z alloys are to be produced via the classical powder metallurgy route of cold pressing plus vacuum sintering and for that blends of the specific powder were mixed, compacted, and consolidated. Fig. 2 shows that the theoretical density of the of the Ti-2X-2Z alloys is higher than that of CP-Ti as all the alloying elements used have higher density compared to Ti. Specifically, the values of the density of the

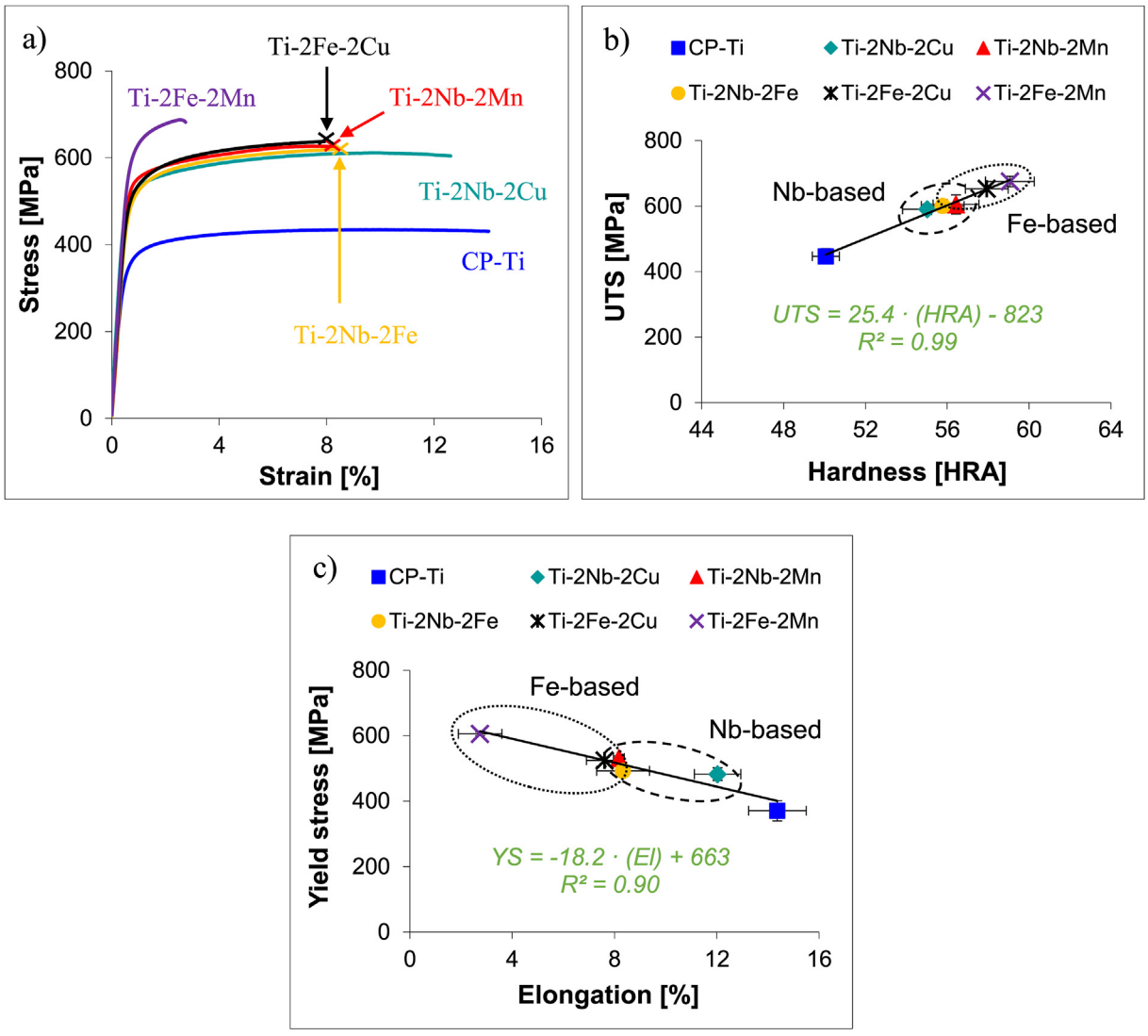

Fig. 5 – Variation of the mechanical properties of the Ti-2X-2Z alloys: a) representative tensile curves, b) ultimate tensile strength vs. hardness, and c) yield stress vs. elongation.

alloying elements, which were used to calculate the theoretical density are: 8.57 g/cm^3 for Nb, 8.96 g/cm^3 for Cu, 7.43 g/cm^3 for Mn, and 7.87 g/cm^3 for Fe. The values of the sintered density of the Ti-2X-2Z alloys are also higher with respect to that of CP-Ti, as they are still a function of the density of the alloying elements, but each actual value is also influenced by the specific diffusivity of the element in Ti. Consequently, a linear relationship between the values of the sintered and theoretical densities is found for the Nb-based Ti-2X-2Z alloys (i.e. Ti–2Nb–2Cu, Ti–2Nb–2Mn, and Ti–2Nb–2Fe) but not for the Fe-based Ti-2X-2Z alloys (i.e. Ti–2Nb–2Fe, Ti–2Fe–2Cu, and Ti–2Fe–2Mn). This is due to the fact that Nb has the highest melting point, and the lowest diffusivity, amongst the alloying elements used and, therefore, it is the element controlling the sintering process when present. In the case of the Fe-based Ti-2X-2Z alloys, no particular element is identified as the limiting one.

A better insight about the effect of the specific alloying element powders used can be gained from the analysis of the relative density values of Fig. 2b). The features of the powder used, including their size, morphology, and deformability, affect the compressibility of the powder blend. Similar or higher compressibility compared to CP-Ti is only achieved in the Ti-2X-2Z alloys containing Cu (i.e. Ti–2Nb–2Cu and Ti–2Fe–2Cu) due to the high deformability of pure Cu. Thus, lower values are obtained for the other Ti-2X-2Z alloys due to the combined effect of the higher hardness of Nb and Mn and the mismatch in particle size for the Fe powder, which has a significantly smaller particle size as well as spherical morphology.

Regardless of the actual relative green density value, it can be noticed that all the Ti-2X-2Z alloys are characterised by a higher value of relative sintered density in comparison to CP-Ti (Fig. 2b), which means that the addition of the selected alloying elements favours the densification of the alloys. Specifically, the Ti–2Nb–2Mn and Ti–2Nb–2Fe alloys reach slightly higher values with respect to the Ti–2Nb–2Cu alloy, even though of the higher relative green density of the latter.

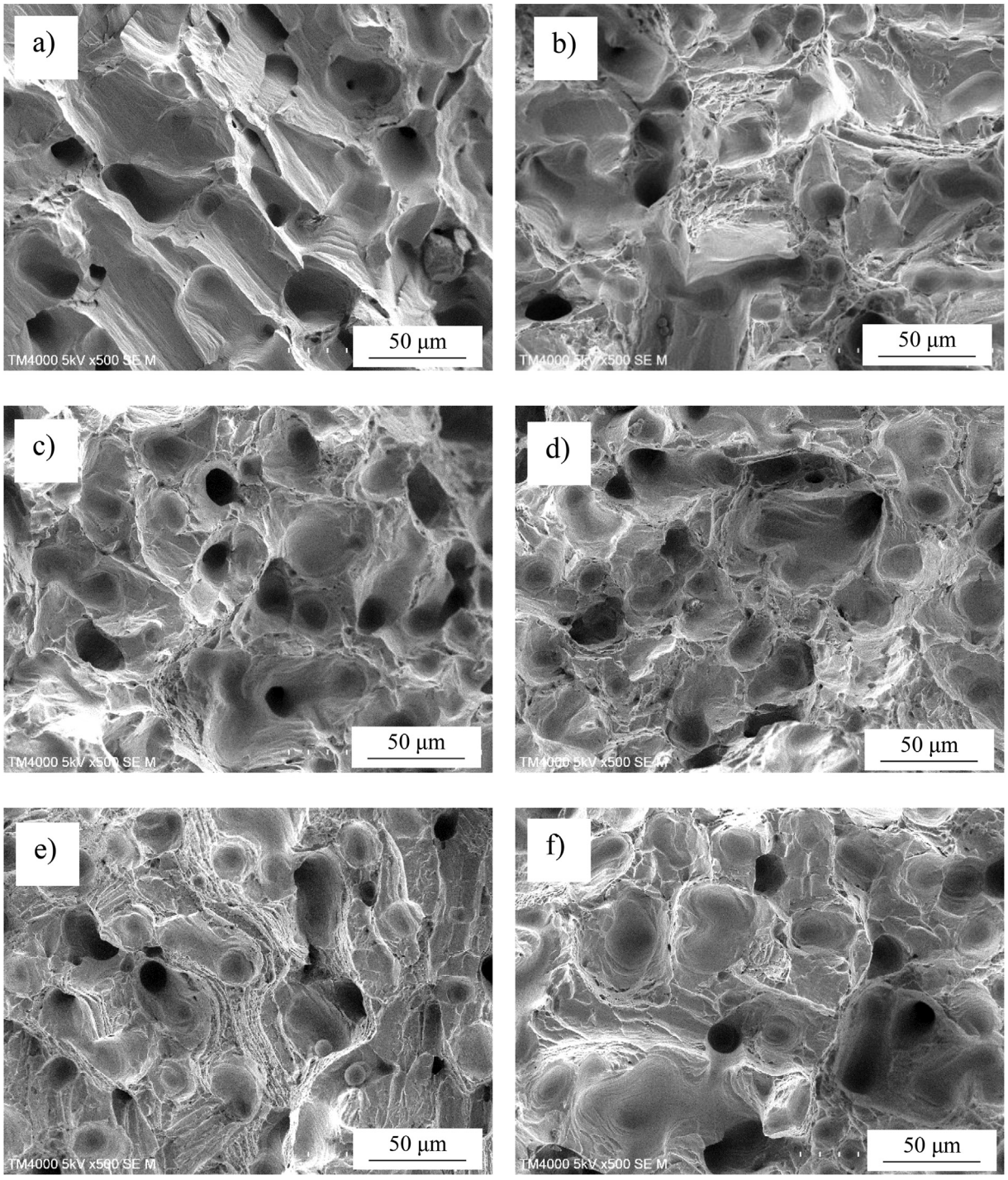

Fig. 6 – Results of the fractographic analysis of the Ti-2X-2Z alloys: a) CP-Ti, b) Ti–2Nb–2Cu, c) Ti–2Nb–2Mn, d) Ti–2Nb–2Fe, e) Ti–2Fe–2Cu, and f) Ti–2Fe–2Mn.

This means that, for the same amount of Nb (i.e. Nb-based Ti-2X-2Z alloys), the addition of Mn or Fe is more beneficial than the addition of Cu, which is due to the intrinsic diffusivity of each element in Ti as well as the fact that the Mn and Fe powders used have smaller particles size compared to Cu. More in detail, the addition of Fe is the most beneficial as it permits to obtain the highest relative sintered density value in the Nb-based Ti-2X-2Z alloys, despite of the lowest relative green density. Considering the Fe-based Ti-2X-2Z alloys allows to highlight two main points. Firstly, Nb is confirmed to be the element slowing down the sintering process, due to its low diffusivity, as the Ti–2Nb–2Fe alloy as the lowest relative sintered density value among the Fe-based Ti-2X-2Z alloys. Secondly, the combined addition of Fe and Mn significantly enhances the sintering process, due to their high diffusivity and small particle size, as the Ti–2Fe–2Mn alloy reaches the

highest relative sintered density value despite starting from the lowest relative green density.

Coherently with the previous discussion about the values of the relative sintered density and the hindering/enhancement of the sintering process, the Ti-2X-2Z alloys have smaller amounts of residual porosity compared to CP-Ti and higher densification. As expected, the Nb-based Ti-2X-2Z alloys have higher porosity and lower densification with respect to the Fe-based Ti-2X-2Z alloys (Fig. 2c). Specifically, for the Nb-based Ti-2X-2Z alloys, a linear reduction of the amount of porosity and a linear increase of the densification is obtained by adding the same amount of Cu→Mn→Fe, and the same linear trends for porosity and densification are obtained for Fe-based Ti-2X-2Z alloys by adding the same amount of Nb→Cu→Mn.

The XRD spectra of Fig. 3 confirm that only the two equilibrium allotropic phases of Ti were found, meaning that the addition of the chosen elements does not lead to the formation of any metastable Ti phases or intermetallic phases. Specifically, exclusively the alpha Ti phase was detected for CP-Ti and the Ti–2Nb–2Cu and Ti–2Fe–2Cu alloys, even though during the microstructural analysis of the latter two the β phase was clearly visible (Fig. 4), which is reflected in the broadening of the α(101) peak. This is due to the fact that the amount of stabilised beta Ti phase is below the detection limit of the equipment. This behaviour is the consequence of the stabilising power of the alloying elements and the microstructure they lead to generate upon slow cooling from a temperature above the β transus of the alloy. In the case of the other Ti-2X-2Z alloys, both the alpha Ti and beta Ti phases were detected where the relative intensity of the main peak of the family of β(110) planes increases with the potency of the β stabiliser element.

Analysis of the microstructure of the studied materials (Fig. 4) reveals that there is a uniform distribution of residual pores left by the sintering process in both CP-Ti and the Ti-2X-2Z alloys, whose volumetric fraction is consistent with the results of the physical properties (Fig. 2). The individual pores have a sphere-shaped morphology and are mainly located at the grain boundaries. These aspects are a confirmation that the materials reached the third stage of sintering during processing, which is associated with the complete dissolution of the powder particles of the alloying elements and achieving a homogenous chemical composition [15,27,29,30,38,44]. This is further confirmed by the fact that no undissolved alloying elements powder particles were found during the microstructural analysis.

Widmanstätten α plates are the only microconstituent of the microstructure of CP-Ti (Fig. 4a–b), which are the result of the allotropic phase transformation of Ti upon furnace cooling under vacuum from the sintering temperature. The addition of a small amount of isomorphous and eutectoid beta stabilisers always switches the plate-like microstructure of CP-Ti to Widmanstätten where its features are affected by the type of alloying elements used. Specifically, the combined addition of Nb (i.e. isomorphous) and Cu (eutectoid) leads to the formation of a coarse Widmanstätten structure composed of elongated α grain boundaries (Fig. 4c) and thick α+β lamellae in the Ti–2Nb–2Cu alloy. The amount of stabilised β is fairly small, as it can be seen from the thin β lamellae (Fig. 4d), which is due to the fact that Nb is soluble in the alpha Ti phase and Cu is a relatively weak β stabiliser (Eq. (1) and Eq. (2)), especially compared to the other eutectoid β stabilisers used in this study.

Swapping the addition of Cu to either Mn (Fig. 4e) or Fe (Fig. 4g) changes the Widmanstätten microstructure of the Nb-based Ti-2X-2Z alloys to being composed of equiaxed α grain boundaries, rather than elongated. More in detail, the addition of Mn or Fe reduces the average size of the α grains and leads to the formation of finer α+β lamellae due to the greater amount of beta Ti phase being stabilised and the fact that neither Mn nor Fe has solubility in the alpha Ti phase at room temperature. The size of the α grains is smaller and the thickness of the β lamellae bigger in the case of the Ti–2Nb–2Mn alloy (Fig. 4f) with respect to the Ti–2Nb–2Fe alloy (Fig. 4h) leading to a more refined Widmanstätten structure. This microstructure is typical of near-α and α+β Ti alloys containing β stabilisers without or with any α stabilisers, and it is created during the slow cooling of the alloy from a temperature above its β transus temperature. Upon crossing this allotropic phase transformation, the beta Ti phase starts to transform into the alpha Ti phase at the grain boundaries and, thus, the equiaxed prior β grains become either elongated or equiaxed α grain boundaries. Nuclei of the alpha Ti phase form with their basal (close-packed) plane parallel to the {110} planes of the beta Ti phase and grow fast along the plane and slow perpendicularly to the plane, generating α lamellae. Depending on the specific solubility of each alloying element, the atoms of the β stabilisers accumulate in the beta Ti phase, stabilising it. The beta Ti phase, therefore, remains within the Widmanstätten structure as β lamellae.

Considering the Fe-based Ti-2X-2Z alloys, the Ti–2Fe–2Cu is characterised by a Widmanstätten structure composed of elongated α grain boundaries (Fig. 4i) and α+β lamellae (Fig. 4j) whose thickness is significantly finer compared to that of the Ti–2Nb–2Cu alloy (Fig. 2d). The Cu-containing Ti-2X-2Z alloys of this study (i.e. Ti–2Nb–2Cu and Ti–2Fe–2Cu) are both characterised by the presence of elongated α grain boundaries, which highlights the weak stabilising power of Cu as eutectoid β stabiliser. The stabilising power of Fe is not sufficiently high to be able to form equiaxed α grain boundaries, which is the case when Mn is simultaneous added to Cu [60]. In the case of the Ti–2Fe–2Mn alloy, due to the high stabilising potency of Fe and Mn, the alloy has the finest Widmanstätten structure amongst the studied Ti-2X-2Z alloys, which is composed of the smallest equiaxed α grain boundaries (Fig. 4k) and the finest α+β lamellae (Fig. 4l). Therefore, in agreement with Eq. (2), rather than Eq. (1), the alloying elements used in this study can be listed in terms of increasing stabilising potency as: Nb→Cu→Fe→Mn.

As discussed in the introduction, the design of new Ti alloys can be done using bond order/d-orbital energy (B_o-M_d) maps [5,6] and the *MoE* parameter [7,8]. These two strategies can also be used to classify Ti alloys along with the standard practise of classifying them based on the phases present in the alloy at room temperature after slow cooling. This should be combined with the knowledge that near-α alloys generally have a maximum of 2–3% of β stabilisers, as this can be used to differentiate them from α+β Ti alloys, which have a higher amount of β stabilisers. From the microstructural analysis

results of the Ti-2X-2Z alloys shown in Fig. 4, alloys which were slow cooled after sintering, it can be assumed that the Cu-containing Ti-2X-2Z alloys (i.e. Ti–2Nb–2Cu and Ti–2Fe–2Cu) are near-α alloys, despite the fact that the total amount of β stabilisers is 4%, due to their coarse Widmanstätten structure and the small amount of stabilised beta Ti phase present in the microstructure. CP-Ti is obviously a α Ti alloy, whereas the other Ti-2X-2Z alloys (i.e. Ti–2Nb–2Mn, Ti–2Nb–2Fe, and Ti–2Fe–2Mn) are α+β Ti alloys as their microstructure is composed of equiaxed grain boundaries and refined α+β lamellae resulting in a fine Widmanstätten structure.

Fig. 7 shows an attempt to classify the Ti-2X-2Z alloys of this study on the basis of the bond order/d-orbital energy (B_o-M_d) map [5,6] and the *MoE* parameter [7,8], respectively. In the case of the bond order/d-orbital energy (B_o-M_d) map (Fig. 7a), the boundaries defining the α (fine dash line) and β (coarse solid line) Ti alloys regions were reported along with the expected change in structure due to the addition of Nb (i.e. coarse dash line). It is found that all the Ti-2X-2Z alloys, with the exception of the Ti–2Fe–2Mn alloy, are classified as α+β Ti alloys as bond order/d-orbital energy (B_o-M_d) maps do not seem to be able to differentiate between near-α and α+β Ti alloys. More in detail, the Ti–2Nb–2Cu alloy lays right in the middle of the α+β Ti alloys region and the Ti–2Fe–2Cu alloy lays very close to the β Ti alloys' border line where, in contrast, microstructural analysis shows that these alloys have a coarse Widmanstätten structure typical of near-α Ti alloys. Even more interestingly, the Ti–2Fe–2Mn alloy is classified as a β Ti alloy, being across the β Ti alloys' border line, but the microstructural analysis clearly shows that the alloy is a α+β Ti alloy characterised by a fine Widmanstätten structure.

Considering the classification of the Ti-2X-2Z alloys of this study on the basis of the *MoE* parameter as calculated per Eq. (1) (i.e. abscissa) and Eq. (2) (i.e. ordinate) shown in Fig. 7b), it can be seen that all the Ti-2X-2Z alloys, with the exception of the Ti–2Nb–2Cu alloy, are classified as near β Ti alloys. As in the case of B_o-M_d) maps, the *MoE* parameter' equations cannot differentiate between near-α and α+β Ti alloys. An interesting case is the Ti–2Nb–2Mn alloy, which is classified as either α+β or near-β Ti alloy, respectively, depending on whether Eq. (1) or Eq. (2) is used as they significantly differ in terms of Mn weighting coefficient. It is worth mentioning that the main source of discrepancy between current theories and the experimental results of this study is most likely related to the cooling rate, as weighting factors of Eq. (1) and Eq. (2) were developed using quenched alloys, whereas the alloys of this study were obtained *via* press and sinter, which is characterised by a slower cooling rate. Therefore, combining the results of this analysis with those of the microstructural characterisation (Fig. 4), it is evident that current theories, especially the *MoE* parameter, are lacking and could be improved to better reflect the stabilisation potency of the different alloying elements, the effect of the processing parameters, and the different type of Ti alloys that can be achieved through their addition.

Regarding the mechanical behaviour, the representative tensile curves of Fig. 5 show that the Ti-2X-2Z alloys as well as CP-Ti do not fail in a catastrophic manner as they are able to deform plastically after the initial elastic deformation. Moreover, as their tensile curves overlay, it can be inferred that the Ti-2X-2Z alloys all have similar elastic modulus, which is comparable to that of CP-Ti. In terms of tensile properties, CP-Ti has the lowest strength and the highest elongation to fracture due to its microstructure composed of Widmanstätten α plates (Fig. 4a–b). Consequently, CP-Ti has also the lowest hardness.

Generally, the combined addition of isomorphous and eutectoid beta stabilisers has a significant effect on the mechanical properties. Specifically, the simultaneous addition of Nb and Cu remarkably increase the strength (i.e. 110 MPa for the yield stress and 140 MPa for the ultimate tensile strength)

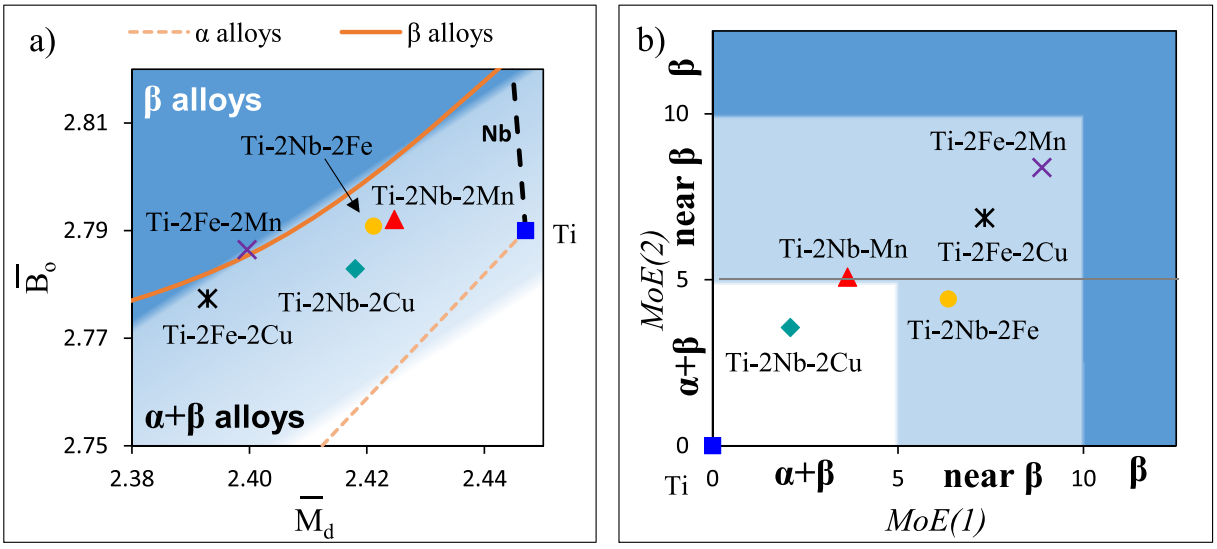

Fig. 7 – Classification of the Ti-2X-2Z alloys by means of current theories: a) bond order/*d*-orbital energy (B_o-M_d) map, and b) *MoE*(1) vs. *MoE*(2).

and hardness with a minor loss of ductility (~2%) as a consequence of the transformation of the microstructure into coarse elongated α grains and thick α+β lamellae (Fig. 4c–d) in the Ti–2Nb–2Cu alloy. The replacement of Cu with Mn or Fe leads to a less significant increase of the strength (~10–50 MPa for both yields tress and ultimate tensile strength where Mn has slightly higher strengthening effect compared to Fe) and hardness but to a comparable loss of ductility (~4%). This behaviour is due to the change of the morphology of the prior β grains to equiaxed, whose size is thus smaller with respect to that of the Ti–2Nb–2Cu alloy, and the reduction of the interlamellar spacing as a consequence of the stabilisation of a greater quantity of β phase (Fig. 4e–h).

It is interesting to note that the Ti–2Fe–2Cu alloy has comparable mechanical properties to those of the Ti–2Nb–2Mn and Ti–2Nb–2Fe alloys as the maximum variation in strength, hardness and elongation among them is, respectively, less than 50 MPa, 2 HRA, and 0.7%. Similar properties are obtained despite the fact that the microstructure of the Ti–2Fe–2Cu alloy is composed of elongated α grains (Fig. 4i–j), rather than equiaxed, and coarse α+β lamellae due to the weak stabilising power of Cu as eutectoid β stabiliser. The combined addition of Fe and Mn results in the Ti–2Fe–2Mn alloy having the highest resistance to plastic deformation during uniaxial load (i.e. tensile) or indentation, and the lowest ability to plastically deform. This behaviour is due to the Ti–2Fe–2Mn alloy being characterised by a more refined Widmanstätten structure constituted by the smallest equiaxed α grains and the finest α+β lamellae (Fig. 4k-l) amongst the studied Ti-2X-2Z alloys. This results in the Ti–2Fe–2Mn alloy having the highest increase of 80 MPa in yield stress and the highest drop of 4.9% in elongation with respect to the group of Ti-2X-2Z alloys with similar mechanical properties (i.e. Ti–2Nb–2Mn, Ti–2Nb–2Fe and Ti–2Fe–2Cu).

It is worth noticing that, generally, higher strength/hardness and lower elongation values are obtained in the Fe-based Ti-2X-2Z alloys with respect to the Nb-based alloys (Fig. 5). This is in agreement with the results of the microstructural characterisation (Fig. 4), and it is a reflection of the stabilising power of the different alloying elements used. Furthermore, from Fig. 5b–c), it can be seen that the variation of the ultimate tensile strength with the hardness and that of the yield stress with the elongation can accurately be expressed as a linear relationship with high coefficients of determination (R^2). Not surprisingly, the linear increase of the ultimate tensile strength is associated with a constant increase of the hardness ($R^2 = 0.99$), and the monotonic increase of the yield stress with a continuous reduction of the ductility ($R^2 = 0.90$).

In terms of failure of the material upon tensile testing (Fig. 6), the fracture surface of CP-Ti is fairly flat, and the material failed through the decohesion at the α grain boundaries even though striation due to the withstood plastic deformation are found within the grains. Moreover, it can be noticed that the residual porosity is highly deformed, transforming into dimples, meaning that the residual pores contributed to the fracture of the material. In general, the fracture surface of the Ti-2X-2Z alloys is rougher with respect to that of CP-Ti and, therefore, tear-ridge like features are present. The Ti-2X-2Z alloys failed through a combination of decohesion at the α grain boundaries and fracture along the α+β lamellae boundaries. Thus, the fracture surface is composed of a majority of flat areas, with striations within them, and a minority of rough areas with step-like appearance. The former are associated with the coarse α lamellae and areas where residual pores were deformed into dimples, and therefore failed in a transgranular ductile manner. The rough areas correspond to the much finer β lamellae and primarily failed intergranularly through the lamellae. In accordance with the microstructural analysis (Fig. 4), the relative amount of rough intergranular areas increases with the refinement of the features (i.e. prior β grain size and interlamellar spacing) of the Widmanstätten structure.

From the fractographic analysis (Fig. 6), the residual porosity left by the sintering process effectively contributes to the failure of the Ti-2X-2Z alloys as pores reduce the actual load bearing cross section and act as stress concentration sites. With the aim of clarifying the relative contribution of the residual porosity, the variation of the mechanical properties of the Ti-2X-2Z alloys as a function of the relative density is plotted in Fig. 8. For powder metallurgy materials, it is expected that a higher relative density results in the monotonic increase of the strength and of the hardness, and in the exponential increase of the ductility as the material approaches full density or zero residual porosity. From the data of Fig. 8, it can be seen that such prediction is correct for the yield stress, the ultimate tensile strength, and the hardness of the Ti-2X-2Z alloys as these three properties are higher for higher values of relative density. Moreover, it can be noticed that the variation of these three properties as a function of the relative density can be estimated through linear relationships which, despite having different coefficients and constants, have comparable R^2 (~0.75). Comprehensively considering the graphs of Figs. 5 and 8, both the microstructural changes induced by the combined addition of different isomorphous and eutectoid beta stabilisers and the reduction of the residual porosity contribute to the enhancement of the strength and of the hardness with respect to CP-Ti. However, the type of combination of alloying elements has a higher strengthening effect than the reduction of the residual porosity.

Regarding the ductility of the Ti-2X-2Z alloys as measured through the elongation to fracture (Fig. 8d), it can be seen that a different trend to the expected is found as the elongation progressively decreases with the increment of the relative density. The actual decreasing trend can effectively be represented with a linear relationship with $R^2 = 0.86$. Holistically, this means that the presence and reduction of the residual porosity has a significantly lower impact on the ductility of the Ti-2X-2Z alloys with respect to the microstructural changes. Specifically, the change of the microstructure of CP-Ti, which is composed of α plates, to a Widmanstätten structure composed of elongated/equiaxed α grains and α+β lamellae through the addition of the selected alloying elements significantly reduces the ability to withstand plastic deformation. This is related to the fact that the movement of the dislocations is much more restricted by the creation of a significantly higher number of grain and lamella boundaries, which have a more negative effect on the ductility than the presence of residual pores. Overall, with respect to the Nb-based Ti-2X-2Z alloys, Fe-based alloys reach higher levels of relative density due to the enhancement of the densification induced by the addition of Fe which results in higher strength (Fig. 8a–b), higher hardness (Fig. 8c) but lower ductility (Fig. 8d).

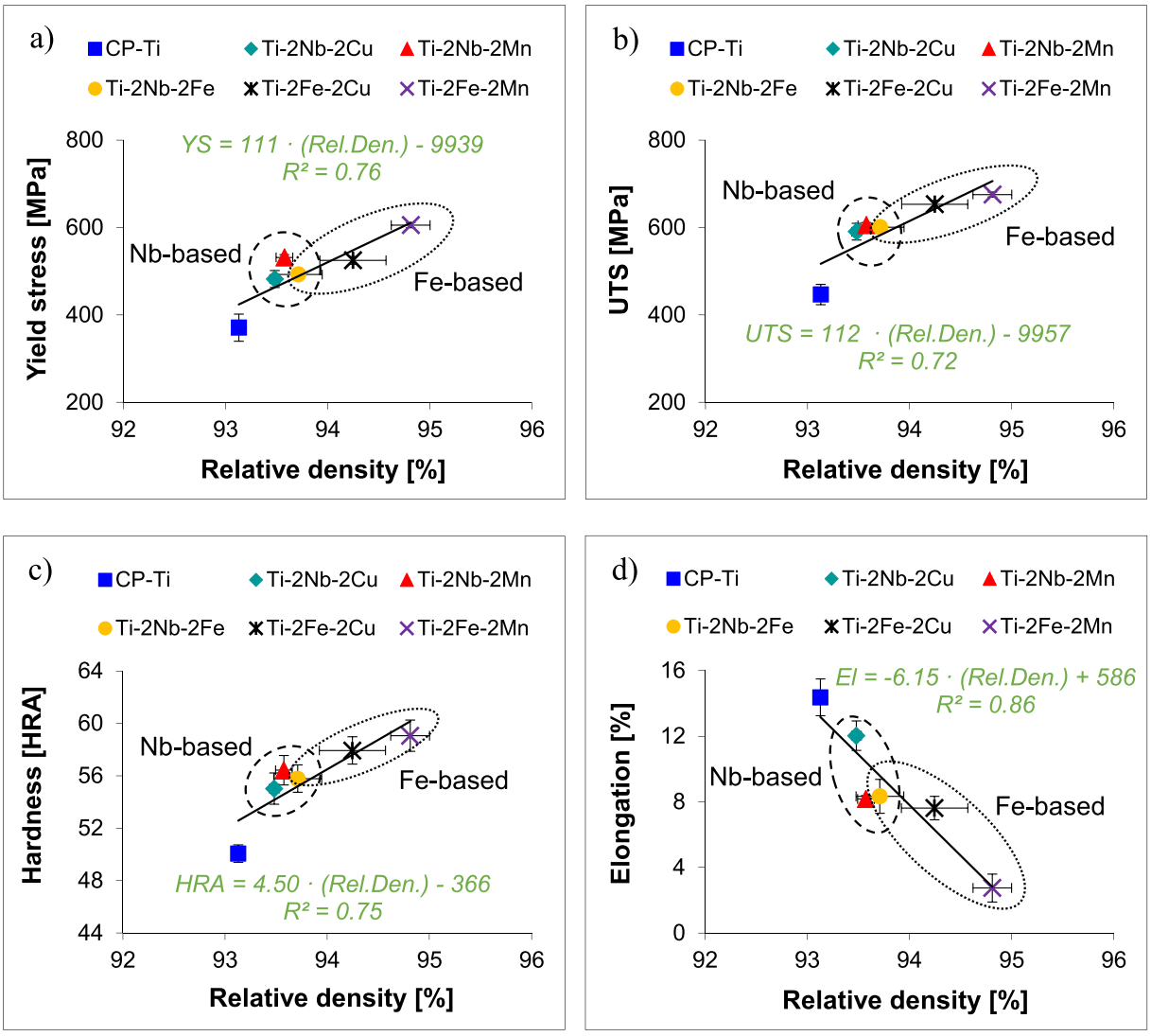

Fig. 8 – Variation of the mechanical properties of the Ti-2X-2Z alloys as a function of the relative density: a) yield stress, b) ultimate tensile strength, c) hardness, and d) elongation.

Fig. 9 shows the variation of the strengthening rate of the Ti-2X-2Z alloys as a function of the true plastic strain where it can be seen that the general behaviour, which reflects the different deformation stages that the alloys undergo, is similar for all the Ti-2X-2Z alloys as the shape of their strengthening curves is alike due to their Widmanstätten microstructure. The strengthening curves can be divided into two segments, the initial sharp decrease of the strengthening rate for true plastic strain below approx. 0.015, which is known as Stage II, and the subsequent reduction of the rate at which the strengthening rate decreases (i.e. Stage III) [61].

In stage II, the Fe-based Ti-2X-2Z alloys have higher strengthening rate compared to CP-Ti and the rest of the Nb-based Ti-2X-2Z alloys whereas in Stage III all the Ti-2X-2Z alloys are characterised by a higher strengthening rate compared to CP-Ti as per the inset in Fig. 9a). This behaviour is the direct consequence of the transformation of the α plates microstructure of CP-Ti into the Widmanstätten microstructure of the Ti-2X-2Z alloys. Particularly, the shape of the strengthening rate curve in Stage III is derived by the compromise between the generation/multiplication and disappearance of dislocations. Therefore, the Ti-2X-2Z alloys are characterised by a higher dislocations generation/multiplication rate whose movement is significantly more hindered by the lamellae boundaries rather than the α plates boundaries.

A detail of the strengthening rate curves in the 0–0.12 true strain range, along with the tensile true stress vs. true strain curves of the Ti-2X-2Z alloys, is shown in Fig. 9b). As per the necking stability Considère criterion [62], the intersection of the two curves of each specific Ti-2X-2Z alloy represents the point at which necking of that alloy during tensile testing starts. For the Ti-2X-2Z alloys, the onset of necking is strongly dependent on the Stage III strengthening rate, and in all the alloys, with the exception of the Ti–2Fe–2Mn alloy, necking is followed by an increase in uniform elongation, which correlates well with the average ductility (Fig. 5), and it is an indication of the toughness of the alloy. More in detail, due to its α plates microstructure characterised by a much lower number

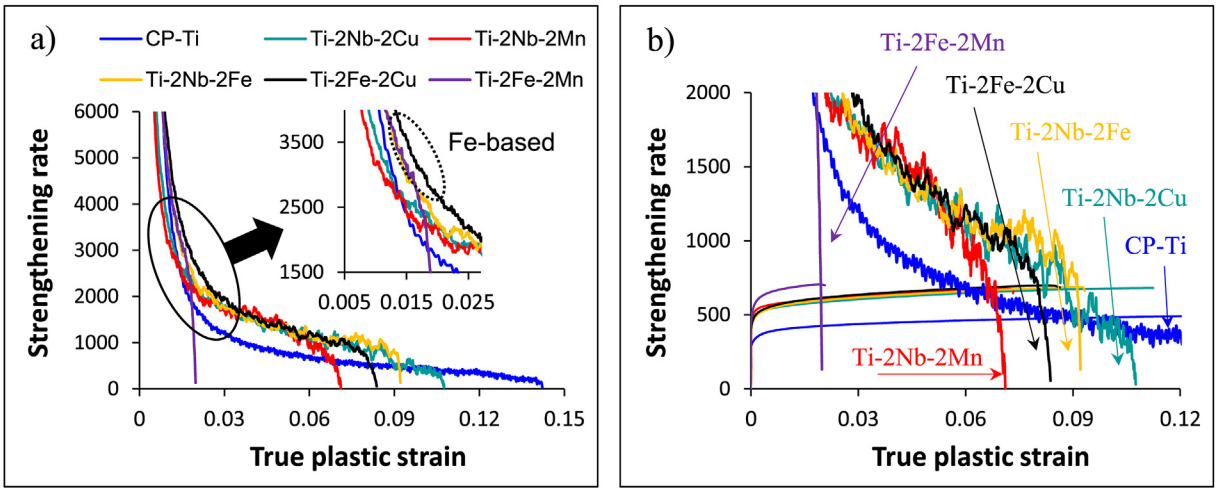

Fig. 9 – Strengthening rate vs. true plastic strain of the Ti-2X-2Z alloys: a) general behaviour, and b) detail of a) including the true stress vs. true strain curves.

of grain boundaries, CP-Ti is able to withstand a significant amount of deformation after necking, resulting in the striation within the α plates found during the fractographic analysis (Fig. 6a). Generally, the finer the Widmanstätten microstructure of the Ti-2X-2Z alloys (i.e. smaller α grains and finer α+β lamellae) the lower the extent of plastic deformation after necking, even though the ductility of the Ti–2Fe–2Cu alloy is lower than that of the Ti–2Nb–2Fe alloy as the former has a greater amount of stabilised β phase as a consequent of bearing two eutectoid beta stabilisers rather than one isomorphous and one eutectoid. In accordance with the tensile curves of Fig. 5, the Ti–2Fe–2Mn alloy fails as the result of neck instability and it is not able to sustain plastic deformation once necking starts.

A comparison of the mechanical behaviour of the Ti-2X-2Z alloys of this study with Ti alloys bearing some of the same alloying elements, and being similar types of Ti alloys, found in literature [20,27,33,40,63] is shown in Fig. 10. From the ultimate tensile strength/hardness pairs, Fig. 10a) shows that, despite of the residual porosity, the Ti-2X-2Z alloys are characterised by better strength and similar hardness to sintered Ti-xCu and wrought Ti-xNb alloys, and higher strength and lower hardness with respect to cast Ti-xCu and cast Ti-xFe alloys. In terms of yield stress/elongation pairs, it can be seen that, most of the Ti-2X-2Z alloys have similar or better yield stress and higher ductility compared to cast Ti-xCu alloys, similar or better yield stress and comparable ductility with respect to wrought Ti-xNb alloys, and similar or better yield stress and lower ductility in comparison to cast Ti-xFe alloys. Moreover, the Ti–2Fe–2Mn alloy has properties comparable to those of the more heavily alloyed cast Ti–4Cu–6Nb alloy. The actual differences between the yield stress/elongation pairs of the Ti-2X-2Z alloys and the other Ti alloys shown in Fig. 10b) are related to the processing method/

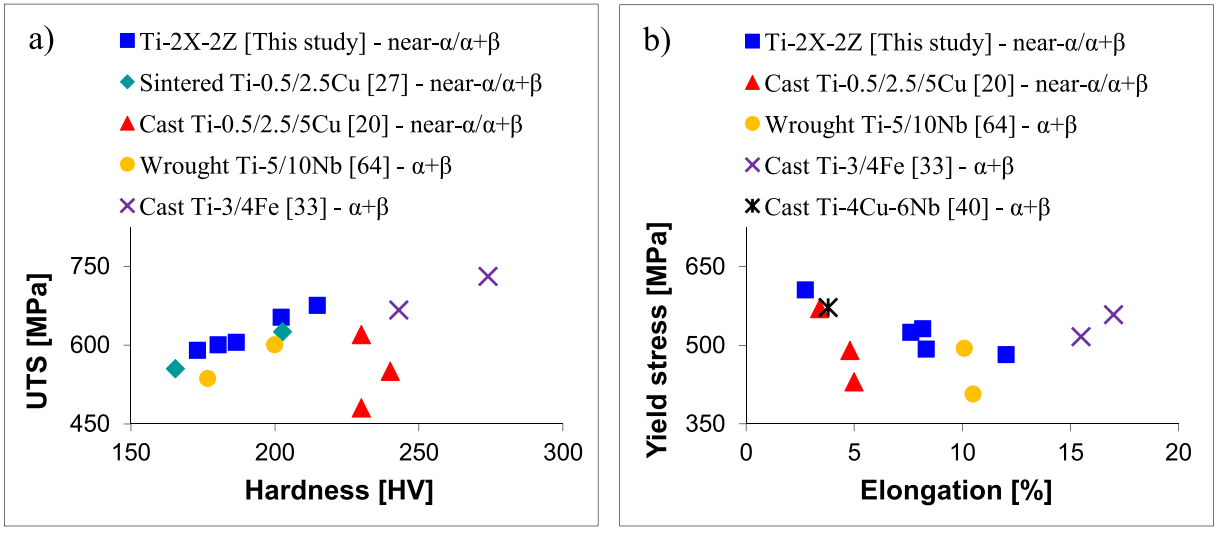

Fig. 10 – Comparison of the mechanical properties of the Ti-2X-2Z alloys of this study with literature [20,27,33,40,63]: a) ultimate tensile strength vs. hardness, and b) yield stress vs. elongation.

conditions and the actual microstructural features deriving from it. Once again, it is worth noticing that the Ti-2X-2Z alloys have similar behaviour to most of the cast/wrought alloys despite bearing a smaller amount of alloying elements and the presence of the residual porosity. This means even better mechanical properties could be achieved in the Ti-2X-2Z alloys through a secondary method like thermomechanical processing or hot isostatic pressing which would seal the residual porosity.

5. Conclusions

In this study a series of Ti-2X-2Z alloys, created through the combined lean additions of isomorphous (i.e. Nb) and eutectoid (i.e. Cu, Mn, and Fe) beta stabilisers, were manufactured aiming to understand the effect of the selected alloying elements on the processability and mechanical behaviour of titanium. As the Ti-2X-2Z alloys were produced via the classical powder metallurgy route of cold pressing plus vacuum sintering it can be concluded that:

- Despite the fact that the addition of the alloying elements reduces the compressibility of the powder blend, higher sintered density values are achieved compared to Ti due to the enhancement of the densification induced by the diffusion of the chosen alloying elements during sintering. The actual enhancement is proportional to the intrinsic diffusivity of the elements and their particle size.
- The addition of the selected isomorphous and eutectoid beta stabilisers does not lead to the formation of any metastable or intermetallic phases and their presence stabilises the beta phase, transforming the microstructure of Ti from α plates to a Widmanstätten structure composed of α grain boundaries and α+β lamellae. The stronger the potency of the beta stabilisers added the more round and smaller the α grains, and the finer the interlamellar spacing.
- Attempting to classify newly developed Ti alloys based on current theories such as bond order/d-orbital energy (B_o-M_d) maps and the molybdenum equivalent (*MoE*) parameter is challenging as they are not able to differentiate between near-α and α+β Ti alloys. Moreover, currently available equations to calculate the *MoE* parameter, which is generally used to design new Ti alloys, are lacking as they do not effectively reflect the stabilisation power of the different alloying elements and the different type of Ti alloys that can be achieved.
- The combined addition of isomorphous and eutectoid beta stabilisers has a significant effect on the mechanical properties and the Ti-2X-2Z alloys fail non-catastrophically through a combination of decohesion at the α grain boundaries and fracture of the α+β lamellae. The strength and hardness increase, and the ductility decreases, as more potent beta stabilisers are used due to the resulting microstructural changes, namely the change of the size and morphology of the prior β grains and the reduction of the size of the α+β lamellae, which have a more significant effect than the reduction of the residual porosity.
- The Ti-2X-2Z alloys have similar strengthening rates and are characterised by similar strengthening mechanisms as they share a Widmanstätten microstructure where the finer the Widmanstätten microstructure the lower the ability to withstand plastic deformation after necking.

Data availability

All metadata pertaining to this work will be made available on request.

Declaration of competing interest

The authors declare that they have no known competing financial interests or personal relationships that could have appeared to influence the work reported in this paper.

Acknowledgements

This work was supported by the New Zealand Ministry of Business, Innovation and Employment (MBIE) through the UOWX1402 research contract.

REFERENCES

[1] Froes FH, Mashl SJ, Moxson VS, Hebeisen JC, Duz VA. The technologies of titanium powder metallurgy. J Occup Med 2004;56:46–8.
[2] Bolzoni L, Nowak M, Hari Babu N. Assessment of the influence of Al-2Nb-2B master alloy on the grain refinement and properties of LM6 (A413) alloy. Mater Sci Eng, A 2015;628:230–7.
[3] Tang B, Chu Y, Zhang M, Meng C, Fan J, Kou H, Li J. The ω phase transformation during the low temperature aging and low rate heating process of metastable β titanium alloys. Mater Chem Phys 2020;239:122125.
[4] Bolzoni L, Ruiz-Navas EM, Gordo E. Influence of vacuum hot-pressing temperature on the microstructure and mechanical properties of Ti-3Al-2.5V alloy obtained by blended elemental and master alloy addition powders. Mater Chem Phys 2012;137:608–16.
[5] Morinaga M, Yukawa N, Maya T, Sone K, Adachi H. Theoretical design of titanium alloys, vol. III. Sixth World Conferecne on Titanium; 1988. p. 1601–6.
[6] Morinaga M. Alloy design based on molecular orbital method. Mater Trans 2016;57:213–26.
[7] Bania PJ. Beta titanium alloys and their role in the titanium industry. J Occup Med 1994;46:16–9.
[8] Wang Q, Dong C, Liaw PK. Structural stabilities of β-Ti alloys studied using a new Mo equivalent derived from [β/(α + β)] phase-boundary slopes. Metall Mater Trans 2015;46:3440–7.
[9] Takeda S, Kakiuchi H, Doi H, Nakamura M. Cytotoxicity of pure metals. Shika Zair Kikai 1989;8:648–52.
[10] Bolzoni L, Ruiz-Navas EM, Gordo E. Investigation of the factors influencing the tensile behaviour of PM Ti-3Al-2.5V alloy. Mater Sci Eng 2014;609:266–72.
[11] Han M-K, Kim J-Y, Hwang M-J, Song H-J, Park Y-J. Effect of Nb on the microstructure, mechanical properties, corrosion behavior, and cytotoxicity of Ti-Nb alloys. Materials 2015;8:5986–6003.
[12] Lee CM, Ju CP, Chern Lin JH. Structure-property relationship of cast Ti-Nb alloys. J Oral Rehabil 2002;29:314–22.

[13] Xu L-J, Xiao S-l, Tian J, Chen Y-y, Huang Y-d. Microstructure and dry wear properties of Ti-Nb alloys for dental prostheses. Trans Nonferrous Metals Soc China 2009;19:s639–44.
[14] Kikuchi M, Takahashi M, Okuno O. Mechanical properties and grindability of dental cast Ti-Nb alloys. Dent Mater J 2003;22:328–42.
[15] Zhao D, Chang K, Ebel T, Qian M, Willumeit R, Yan M, Pyczak F. Microstructure and mechanical behavior of metal injection molded Ti-Nb binary alloys as biomedical material. J Mech Behav Biomed Mater 2013;28:171–82.
[16] Yılmaz E, Gökçe A, Findik F, Gulsoy HO. Metallurgical properties and biomimetic HA deposition performance of Ti-Nb PIM alloys. J Alloys Compd 2018;746:301–13.
[17] Kalita D, Rogal Ł, Czeppe T, Wójcik A, Kolano-Burian A, Zackiewicz P, Kania B, Dutkiewicz J. Microstructure and mechanical properties of Ti-Nb alloys prepared by mechanical alloying and spark plasma sintering. J Mater Eng Perform 2020;29:1445–52.
[18] Ohkubo C, Shimura I, Aoki T, Hanatani S, Hosoi T, Hattori M, Oda Y, Okabe T. Wear resistance of experimental Ti-Cu alloys. Biomaterials 2003;24:3377–81.
[19] Zhu KY, Zhao YQ, Qu HL, Wu ZL, Zhao XM. Microstructure and properties of burn-resistant Ti-Al-Cu alloys. J Mater Sci 2000;35:5609–12.
[20] Kikuchi M, Takada Y, Kiyosue S, Yoda M, Woldu M, Cai Z, Okuno O, Okabe T. Mechanical properties and microstructures of cast Ti-Cu alloys. Dent Mater 2003;19:174–81.
[21] Zhang E, Ren J, Li S, Yang L, Qin G. Optimization of mechanical properties, biocorrosion properties and antibacterial properties of as-cast Ti-Cu alloys. Biomed Mater 2016;11:065001.
[22] Yi CB, Ke ZY, Zhang L, Tan J, Jiang YH, He ZY. Antibacterial Ti-Cu alloy with enhanced mechanical properties as implant applications. Mater Res Express 2020;7:105404.
[23] Zhang E, Wang X, Chen M, Hou B. Effect of the existing form of Cu element on the mechanical properties, bio-corrosion and antibacterial properties of Ti-Cu alloys for biomedical application. Mater Sci Eng C 2016;69:1210–21.
[24] Wang J, Zhang S, Sun Z, Wang H, Ren L, Yang K. Optimization of mechanical property, antibacterial property and corrosion resistance of Ti-Cu alloy for dental implant. J Mater Sci Technol 2019;35:2336–44.
[25] Zhang E, Li S, Ren J, Zhang L, Han Y. Effect of extrusion processing on the microstructure, mechanical properties, biocorrosion properties and antibacterial properties of Ti-Cu sintered alloys. Mater Sci Eng C 2016;69:760–8.
[26] Liu J, Li F, Liu C, Wang H, Ren B, Yang K, Zhang E. Effect of Cu content on the antibacterial activity of titanium-copper sintered alloys. Mater Sci Eng C 2014;35:392–400.
[27] Alshammari Y, Yang F, Bolzoni L. Low-cost powder metallurgy Ti-Cu alloys as a potential antibacterial material. J Mech Behav Biomed Mater 2019;95:232–9.
[28] Alshammari Y, Jia M, Yang F, Bolzoni L. The effect of $\alpha+\beta$ forging on the mechanical properties and microstructure of binary titanium alloys produced via a cost-effective powder metallurgy route. Mater Sci Eng, A 2020;769:138496.
[29] Chen B-Y, Hwang K-S, Ng K-L. Effect of cooling process on the alpha phase formation and mechanical properties of sintered Ti-Fe alloys. Mater Sci Eng, A 2011;528:4556–63.
[30] Raynova S, Imam MA, Yang F, Bolzoni L. Hybrid microwave sintering of blended elemental Ti alloys. J Manuf Process 2019;39:52–7.
[31] Romero C, Yang F, Raynova S, Bolzoni L. Thermomechanically processed powder metallurgy Ti-5Fe alloy: effect of microstructure, texture, Fe partitioning and residual porosity on tensile and fatigue behaviour. Materialia 2021;20:101254.
[32] Romero C, Yang F, Wei S, Bolzoni L. Thermomechanical processing of cost-affordable powder metallurgy Ti-5Fe alloys from the blended elemental approach: microstructure, tensile deformation behavior, and failure. Metals 2020;10:1–16.
[33] Niu J, Guo Y, Li K, Liu W, Dan Z, Sun Z, Chang H, Zhou L. Improved mechanical, bio-corrosion properties and in vitro cell responses of Ti-Fe alloys as candidate dental implants. Mater Sci Eng C 2021;122:111917.
[34] Chen B-Y, Hwang K-S. Sintered Ti-Fe alloys with in situ synthesized TiC dispersoids. Mater Sci Eng, A 2012;541:88–97.
[35] Esteban PG, Bolzoni L, Ruiz-Navas EM, Gordo E. PM processing and characterisation of Ti-7Fe low cost titanium alloys. Powder Metall 2011;54:242–52.
[36] Gouda MK, Nakamura K, Gepreel MAH. Effect of Mn-content on the deformation behavior of binary Ti-Mn alloys. Key Eng Mater 2016;705:214–8.
[37] Cho K, Niinomi M, Nakai M, Hieda J, Fernandes Santos P, Itoh Y, Ikeda M. Mechanical properties, microstructures, and biocompatibility of low-cost β-type Ti-Mn alloys for biomedical applications. Biomater Sci: Processing, Properties and Applications IV 2014;251:21–30.
[38] Fernandes Santos P, Niinomi M, Liu H, Cho K, Nakai M, Itoh Y, Narushima T, Ikeda M. Fabrication of low-cost beta-type Ti-Mn alloys for biomedical applications by metal injection molding process and their mechanical properties. J Mech Behav Biomed Mater 2016;59:497–507.
[39] Kim J-W, Hwang M-J, Han M-K, Kim Y-G, Song H-J, Park Y-J. Effect of manganese on the microstructure, mechanical properties and corrosion behavior of titanium alloys. Mater Chem Phys 2016;180:341–8.
[40] Takahashi M, Kikuchi M, Takada Y. Mechanical properties and microstructures of dental cast Ti-6Nb-4Cu, Ti-18Nb-2Cu, and Ti-24Nb-1Cu alloys. Dent Mater J 2016;35:564–70.
[41] Mutlu I, Oktay E. Localised corrosion behaviour of biomedical implant materials using electrochemical potentiokinetic reactivation and critical pitting potential methods, corrosion engineering. Sci Technol 2015;50:72–9.
[42] Sato K, Takahashi M, Takada Y. Construction of Ti-Nb-Ti2Cu pseudo-ternary phase diagram. Dent Mater J 2020;39:422–8.
[43] Chen Z, Liu Y, Jiang H, Liu M, Wang CH, Cao GH. Microstructures and mechanical properties of Mn modified, Ti-Nb-based alloys. J Alloys Compd 2017;723:1091–7.
[44] Ehtemam-Haghighi S, Attar H, Dargusch MS, Kent D. Microstructure, phase composition and mechanical properties of new, low cost Ti-Mn-Nb alloys for biomedical applications. J Alloys Compd 2019;787:570–7.
[45] Hsu H-C, Hsu S-K, Wu S-C, Lee C-J, Ho W-F. Structure and mechanical properties of as-cast Ti-5Nb-xFe alloys. Mater Char 2010;61:851–8.
[46] Ehtemam-Haghighi S, Liu Y, Cao G, Zhang L-C. Phase transition, microstructural evolution and mechanical properties of Ti-Nb-Fe alloys induced by Fe addition. Mater Des 2016;97:279–86.
[47] Ehtemam-Haghighi S, Liu Y, Cao G, Zhang L-C. Influence of Nb on the $\beta \rightarrow \alpha''$ martensitic phase transformation and properties of the newly designed Ti-Fe-Nb alloys. Mater Sci Eng C 2016;60:503–10.
[48] Ehtemam-Haghighi S, Prashanth KG, Attar H, Chaubey AK, Cao GH, Zhang LC. Evaluation of mechanical and wear properties of TixNb7Fe alloys designed for biomedical applications. Mater Des 2016;111:592–9.
[49] Afonso CRM, Chaves JM, Florêncio O. Effect of rapid solidification on microstructure and elastic modulus of β Ti-

xNb-3Fe alloys for implant applications. Adv Eng Mater 2017;19:1600370.
[50] Li Q, Miao P, Li J, He M, Nakai M, Niinomi M, Chiba A, Nakano T, Liu X, Zhou K, Pan D. Effect of Nb content on microstructures and mechanical properties of Ti-xNb-2Fe alloys. J Mater Eng Perform 2019;28:5501–8.
[51] Salvador CAF, Dal Bó MR, Costa FH, Taipina MO, Lopes ESN, Caram R. Solute lean Ti-Nb-Fe alloys: an exploratory study. J Mech Behav Biomed Mater 2017;65:761–9.
[52] Chirico C, Tsipas SA, Wilczynski P, Gordo E. Beta titanium alloys produced from titanium hydride: effect of alloying elements on titanium hydride decomposition. Metals 2020;10.
[53] Cho K, Niinomi M, Nakai M, Hieda J, Kawasaki Y. Development of high modulus Ti-Fe-Cu alloys for biomedical applications. Mater Trans 2013;54:574–81.
[54] Zadorozhnyy VY, Inoue A, Louzguine-Luzgin DV. Ti-Based nanostructured low-alloy with high strength and ductility. Mater Sci Eng, A 2012;551:82–6.
[55] Zadorozhnyy VY, Shi X, Kozak DS, Wada T, Wang JQ, Kato H, Louzguine-Luzgin DV. Electrochemical behavior and biocompatibility of Ti-Fe-Cu alloy with high strength and ductility. J Alloys Compd 2017;707:291–7.
[56] Chaussê de Freitas C, Campo KN, Caram R. Thixoforming of titanium: the microstructure and processability of semisolid Ti-Cu-Fe alloys. Vacuum 2020;180:109567.
[57] Ikeda M, Ueda M, Kinoshita T, Ogawa M, Niinomi M. Influence of Fe content of Ti-Mn-Fe alloys on phase constitution and heat treatment behavior. Mater Sci Forum 2012;706–709:1893–8.
[58] Raynova S, Collas Y, Yang F, Bolzoni L. Advancement in the pressureless sintering of CP titanium using high-frequency induction heating. Metall Mater Trans 2019;50:4732–42.
[59] Wang H, Fang ZZ, Sun P. A critical review of mechanical properties of powder metallurgy titanium. Int J Powder Metall 2010;46:45–57.
[60] Bolzoni L, Alqattan M, Peters L, Alshammari Y, Yang F. Ternary Ti alloys functionalised with antibacterial activity. Sci Rep 2020;10:22201.
[61] Kocks UF, Mecking H. Physics and phenomenology of strain hardening: the FCC case. Prog Mater Sci 2003;48:171–273.
[62] Weber L, Kouzeli M, San Marchi C, Mortensen A. On the use of considere's criterion in tensile testing of materials which accumulate internal damage. Scripta Mater 1999;41:549–51.
[63] Zhang Y, Sun D, Cheng J, Tsoi JKH, Chen J. Mechanical and biological properties of Ti-(0-25 wt%)Nb alloys for biomedical implants application. Regenerative Biomaterials 2020;7:119–27.